

## Statement

This manuscript has been submitted for publication in the Geophysics (SEG). The article has not yet been peer reviewed, and subsequent versions of this manuscript may be different. If accepted, the final version of this manuscript will be available via the ‘Peer reviewed Publication DOI’ link on the right-hand side of this webpage. Please feel free to contact the corresponding author, we welcome feedback.

# Uncertainty quantification of multi-modal surface wave inversion using artificial neural networks

Alexandr Yablokov<sup>1,2,3,\*</sup>, Yevgeniya Lugovtsova<sup>4</sup>, Aleksander Serdyukov<sup>1,2,3</sup>

<sup>1</sup>*Trofimuk Institute of Petroleum Geology and Geophysics of Siberian Branch of the Russian Academy of Sciences (IPGG SB RAS), Novosibirsk, Russia.*

<sup>2</sup>*Chinakal Institute of Mining of Siberian Branch of the Russian Academy of Sciences, Novosibirsk, Russia.*

<sup>3</sup>*Novosibirsk State University, Novosibirsk, Russia.*

<sup>4</sup>*Bundesanstalt für Materialforschung und -prüfung, Berlin, Germany.*

\**E-mail of corresponding author: yablokovav@ipgg.sbras.ru*

(April 29, 2022)

Running head: **Uncertainties of multi-modal inversion**

# ABSTRACT

**Keywords:** surface wave dispersion curves, artificial neural network, inversion

An inversion of surface waves dispersion curves is a non-unique and ill-conditioned problem. The inversion result has a probabilistic nature, what becomes apparent when simultaneously restoring the shear wave (S-wave) velocity and layer thickness. Therefore, the problem of uncertainty quantification is relevant. Existing methods through deterministic or global optimization approaches of uncertainty quantification via posterior probability density (PPD) of the model parameters are not computationally efficient since they demand multiple solutions of the inverse problem. We present an alternative method based on a multi-layer fully connected artificial neural network (ANN). We improve the previous approach from uni-modal to multi-modal inversion and use the existing algorithm to determine optimal parametrization (number of layers) and the ranges of possible model parameters. We uniformly draw training data sets within estimated ranges and train the ANN. Saved ANN's weights map the phase velocity dispersion curves to values of the S-wave velocity and layers thickness. To estimate the uncertainties, we adapt the Monte-Carlo simulation strategy and project onto the resulting velocity model both frequency-dependent data noise and inverse operator errors, which are evaluated by the prediction of the training data set. We first test our approach on synthetic experiments for various velocity models: a positive velocity gradient, a low-velocity layer and a high-velocity layer. This is done considering uni-modal inversion at first and then compared to the multi-modal inversion. Afterwards, we apply our approach to field data and compare resulting models with

the body S-wave processing by the generalized reciprocal method. The experiments show high-potential results - using ANN yields the possibility to accurately estimate PPD of restored model parameters without a significant computational effort. The PPD-based comparison demonstrates advantages of a multi-modal inversion over uni-modal inversion. The trained ANN provides reasonable model parameters predictions and related uncertainties in real-time.

## INTRODUCTION

A method of multichannel analysis of surface waves (MASW) is widely used to study near surface geological structures for several decades (Park et al., 1999). We consider a key MASW problem of simultaneous inversion of surface wave phase velocity dispersion curves (DCs) for shear wave (S-wave) velocities and layer thicknesses, which are the parameters of the layered near surface model (Miller et al., 1999). Note, that the simultaneous inversion for both of the parameters is much more challenging than looking only for unknown velocities for a fixed layer depth velocity model, which was considered in a number of earlier MASW studies. Global search methods (Cox and Teague, 2016; Song et al., 2015), Monte Carlo inversion and artificial neural network (ANN) (Çaylak and Kaftan, 2014; Yablokov and Serdyukov, 2020) were previously implemented for determination of both the unknown velocities and layer thicknesses. As an alternative, Cao et al. (2020) proposed to split the velocity model into several depth intervals and determine the averaged  $V_s$  values for each interval from DCs data by mixed density neural networks (MDN). Aleardi and Stucchi (2021) train a residual neural network (ResNet) to map the spectral dispersion image of the surface wave into S-wave velocity and layer thicknesses. The advantages of using artificial neural networks (ANN) are higher computational efficiency without a need to adjust optimization parameters and the lack of necessity to include any model constraint into the error function, unlike global optimization methods (Yablokov and Serdyukov, 2020; Aleardi and Stucchi, 2021; Yablokov et al., 2021).

The inversion of surface wave DCs for S-wave velocity model parameters is an

ill-posed problem (Foti et al., 2014). In particular, the ambiguity of the DCs inversion increases with the number of recovered velocity model parameters. The solution should be considered in a probabilistic sense, which leads to a problem of estimation of the uncertainties of the surface wave DCs inversion. The first uncertainty studies related to the surface wave analysis were focused on the estimation of the dispersion data errors, studying data from repetitive filed data gathering experiments (Marosi and Hiltunen, 2004) and propagating these errors by local optimisation inversion method onto model uncertainties (Lai et al., 2005). However, these researchers did not take into account the ill-posedness of the surface wave data inversion. Comina et al. (2011) and Foti et al. (2009) used a Monte Carlo approach to select a set of S-wave velocity models that can be considered equivalent with respect to fitting DCs according to the experimental uncertainties. This set of equivalent solutions is then used to evaluate the resulting model uncertainty. Molnar et al. (2010) employed a Bayesian framework and Markov Chain Monte Carlo (MCMC) method to cast the surface wave DCs data inversion into a solid probabilistic statement for accurate estimation of a posterior probability density (PPD). Aleardi et al. (2020) performed a rigorous study and comparison of transdimensional and reversible-jump MCMC inversions of Rayleigh-wave DCs. Aleardi and Stucchi (2021) state MCMC methods are computationally expensive due to the huge number of samples needed to attain stable PPDs. For this reason, the MCMC approach becomes computationally impractical for inverting big data. Aleardi and Stucchi (2021) considered the machine learning based inversion of a full dispersion images and suggested a Monte Carlo simulation strategy that propagates onto the model space the uncertainties related to noise in

the data and the modelling error introduced by the network approximation.

To reduce the ambiguity in the estimated model parameters, it is advantageous to use multiple modes in the inversion procedure (Beatty et al., 2002; Xia et al., 2003). Luo et al. (2007) found that the relative error in the velocity estimation decreases from 16% when only the fundamental mode is used to 4% when the fundamental mode as well as the first two higher-order modes are used in the inversion. Supranata et al. (2007) concluded that a more accurate inversion of irregular velocity profiles can be achieved when higher-order modes are included. The main problem to deal with is the separation and identification of different modes in the spectrum. Zhang and Chan (2003) state that mode-misidentification errors on the experimental DCs are often greater than errors resulting from inaccurate data for a given mode. An inversion of the full dispersion image of the surface wave (Aleari and Stucchi, 2021) seems a reasonable alternative to the multiple-mode inversion. This approach is based on a full surface wavefield modelling, which is challenging due to the need to take into account attenuation, scattering of the surface waves, the presence of other types of waves and unknown source wavelet as well. A standard reflectively approach and isotropic stratified elastic medium is not suitable for near surface full wave form modelling in practice. At least, one has to define unknown pressure wave velocity ( $V_P$ ) and density ( $\rho$ ) values which affect the modelling waveforms but typically not determined via the MASW method. The DCs are much less sensitive to these parameters. From this point, the DCs-based multi-mode inversion seems to be a more solid approach. Also, there are approaches dealing with the problems of higher modes picking and misiden-

tification. Maraschini et al. (2010) proposed an inversion procedure was defined in a way that several modes could be taken into account simultaneously and there was no need for identifying the modes. Recently, Serdyukov et al. (2019) demonstrated that the slant f-k transform (SFK) provides well-traced spectral multiple-mode images even in cases when standard 2D time-spacial Fourier transform technique (which is actually equivalent to phase-shift (Park et al., 1999) and some other popular spectral processing methods) enables the selection only of one fundamental mode for the subsequent inversion.

In this contribution, we follow the ANN method for the surface wave fundamental mode DCs inversion for S-wave velocity and layer thicknesses suggested by Yablokov et al. (2021) and further develop their approach for the multiple mode DCs inversion. First, we define the optimal parametrization (number of layers of restoring velocity model) and possible near-surface parameter ranges for the layered model based on the observed frequency-dependended phase velocity. Then we prepare a training data set by generating numerous random layered models by uniform distribution over the determined parameter intervals and computing DCs using fast parallel forward solver. Due to the verified data-driven approach offered by Yablokov et al. (2021), the ANN is trained on a data set containing realistic subsurface scenarios and learns how to reproduce a similar velocity model to fit the input multiple mode DCs data. At current research, we use the rigorous adjusted ANN architecture and parameters proposed by Yablokov et al. (2021). The pre-trained ANN enables one to project dispersion data noise and inverse operator errors onto a space of the velocity model parameters.

Thus, we adapt the Monte-Carlo simulation strategy applied by Aleardi and Stucchi (2021) to estimate uncertainties of our ANN multiple DCs inversion method.

The paper is organized into three main sections, covering methodology, synthetic and field examples, and discussion. In the methodology section, we provide the details of the proposed algorithms: ANN inversion and Monte-Carlo simulation strategy. In the second section, "Results", we first test our approach on synthetic experiments for various velocity models: a positive velocity gradient, a low-velocity layer, and a high-velocity layer and compare uni- and multi-modal inversion cases. Then, we apply the ANN inversion and uncertainty estimation strategy to field data. We compare resulting models with body S-wave processing by the generalized reciprocal method. In the last section, "Discussions", we resume the main point, sum up time computing and refer to some aspects, which are not mentioned in the paper.

## METHODS

The near surface seismic exploration by multichannel analysis of surface wave method (MASW), which is considered in the paper, includes following steps: (i) surface waves data acquisition using linear profiles, (ii) spectral analysis for phase velocity dispersion curves (DCs) extraction, (iii) an inversion of the extracted phase velocities into the S-wave velocity model.

## The dispersion curves extracting and data structure

We use the slant f-k (SFk) transform (Serdyukov et al., 2019) to compute phase-velocity ( $V - f$ ) spectra of the surface waves. Next, we manually pick and extract dispersion curves of several first modes from the computed SFk  $V - f$  spectral image. The SFk transform provides much more clear spectral images of the surface waves, compared with standard methods such as 2D Fourier transform f-k or phase shift method (Serdyukov et al., 2019), that enables an observation of the higher modes.

We compose an input data vector from the selected DCs in order of increasing the frequency and the mode number. Let us denote a mode and frequency sample numbers by indexes  $i = 1 \dots N$  and,  $j = 1 \dots M$  respectively. Each pair of indexes  $ij$  spawns an index  $k = i + (j - 1)N$ . The corresponding  $k$ -th element of a resulting input data vector  $\mathbf{V}_R^{input}$  is a value of the phase velocity of  $i$ -th mode of the Rayleigh wave for the  $j$ -th sample frequency. Note that typically the fundamental mode is referred to the zero mode and the first mode is the first higher order mode. However, here, for simplicity, we will enumerate surface wave modes from the fundamental mode starting with one ( $i = 1$ ). Since high order modes ( $i > 1$ ) do not exist below some frequency, we fill the missing elements of the input data vector with zeros. This is done because the same length for all modes is necessary for further processing.

## The inversion algorithm based on an artificial neural network

We follow the artificial neural network (ANN) inversion algorithm described by Yablokov et al. (2021). We have improved it from a uni-modal to a multi-modal approach. The DCs inversion consists of the following steps: (1) estimation of the ranges of the velocity model parameters by an averaged fundamental mode DC; (2) calculation of a training data set for a predetermined number of modes; (3) Creation and training the ANN (4) application of the ANN for the inversion of the multiple-mode surface wave DCs.

At the first step of the ANN inversion, we follow Cox and Teague (2016) and set the ranges of  $V_S$  and  $h$  to define the space of possible layered models. We use only the fundamental mode DC, since the fundamental mode has the highest penetration depth compared to all other modes. Yablokov et al. (2021) demonstrate this approach is suitable for such rough preliminary estimations. A number of layers,  $l$ , is also defined at this step.

At the second step, we define the ANN training data set. We select a number, i.e. a set  $\{\mathbf{V}_S, \mathbf{h}\}$  of S-wave model vectors  $\mathbf{V}_S = (V_S^1, V_S^2, \dots, V_S^l)$  and thickness  $\mathbf{h} = (h^1, h^2, \dots, h^{l-1})$  assuming the uniform distribution of both parameters over the previously defined intervals (the ranges from the first step). Each pair of  $[\mathbf{V}_S, \mathbf{h}]$  is a model sample vector, which is an element of the matrix of the training models dataset  $\mathbf{M}^{train}$ . Next, we calculate the matrix  $\mathbf{D}^{train} = \{\mathbf{V}_R^{train}\}$  which contains the corresponding number of training data DCs vectors by the numerical solution of

Rayleigh wave dispersion equation (Herrmann, 2013). P-wave velocities, which are needed to calculate DCs, are obtained from equation:  $V_P = V_S \sqrt{2(1 - \nu)/(1 - 2\nu)}$ , where the Poisson’s ratio  $\nu$  is assumed to be equal to 0.35. We also use empirical ratio for the density:  $\rho = 2.35 + 0.036 * (\mathbf{V}_P - 3)^2 \text{ g/cm}^3$  (Kurita, 1973). The dispersion equation numerical solver was coded in Python using the ”Numba” library (<https://github.com/keurfonluu/disba>) and parallelized on CPUs. This allows extremely fast calculation of DCs. For example, it takes about 0.0055 s to calculate the fundamental mode DC for a four-layer velocity model for 100 frequencies samples. The structure of each resulting multi-mode DCs training data vector  $\mathbf{V}_R^{train}$  from the matrix  $\mathbf{D}^{train}$  is the same as the structure of the input data vector  $\mathbf{V}_R^{input}$ , which was given above in the paper.

At the third step, the ANN is created and trained. We follow Yablokov et al. (2021) and perform the same studies to design an optimal ANN architecture. Here we skip these details - the results are similar to those, presented in (Yablokov et al., 2021). The ANN input layer is composed of  $n \times m$  neurons and is designed according to the structure of input data  $\mathbf{V}_R^{input}$ . The ANN output layer is designed to produce the concatenation of vectors  $[\mathbf{V}_S, \mathbf{h}]$  of the length  $2l - 1$ , representing the resulting velocity model. The number of sample models in  $\mathbf{M}^{train}$  is selected equal to 100,000 and there is the same number of multi-modal DC data vectors in  $\mathbf{D}^{train}$ . The ANN weights are obtained by the minimization of a misfit function:

$$\text{MAE}(\mathbf{W}(\mathbf{V}_R^{train}) - [\mathbf{V}_S, \mathbf{h}]) \rightarrow \min, \quad (1)$$

where MAE is the mean absolute error and  $\mathbf{W}$  is ANN action with fitted weights,

i.e. an inverse operator that maps the domain of the picked phase velocities into the domain of the model parameters:

$$\mathbf{W}(\mathbf{V}_R) = [\mathbf{V}_S, \mathbf{h}]. \quad (2)$$

## Uncertainty quantification with a Monte Carlo simulation

We adapted the Monte Carlo simulation strategy by Aleari and Salusti (2021) and apply it for the uncertainty quantification of the MASW method results. To estimate uncertainties, both dispersion data noise and inverse operator errors have to be projected onto a space of the velocity model parameters.

The statistical characteristics of the dispersion data noise are determined based on the  $V - f$  amplitude spectrum of the data. The standard deviation ( $\sigma$ ) of the noise in the phase velocity values (e.i the picked DC) should be frequency-variant ( $\sigma_{noise}(f)$ ) since the spectral smearing increases with decreasing frequency. To introduce the picking errors, at first, a phase velocity range within which a picking error can occur is set. The confidence interval (for example, shown in Figure 1b by red lines) is limited to the points at which the spectral amplitudes of a mode are decreased twice relative to its maximum at a fixed frequency. This is done for each mode. Let us denote the resulting phase velocity vector as  $\mathbf{V}_R^{extracted}(f)$ . The confidence interval length is supposed to be equal to  $6\sigma$ . Let us assume that the distribution of noise at each frequency is symmetric around the maximum value and accept the expected value  $\mu_{noise}(f) = 0$ . On these assumptions, we propose to introduce normally distributed noise  $N^{noise}(0, \sigma_{noise}(f))$  into phase velocity values of dispersion curves at

each frequency.

To determine inverse operator errors, we apply the trained ANN to invert all dispersion curves from the dataset  $\mathbf{D}^{train}$ :

$$\mathbf{W}(\mathbf{D}) = \overline{\mathbf{M}}. \quad (3)$$

Then we estimate the errors connected to the reconstruction of the model parameters:

$$\mathbf{E} = \mathbf{M}^{train} - \overline{\mathbf{M}} \quad (4)$$

We assume that the errors of the inverse operator,  $N^{error}(\mu_{error}, \sigma_{error})$ , are normally distributed for the estimation of the expected value  $\mu_{error}$  and the standard deviation  $\sigma_{error}$  of  $\mathbf{E}$ .

After the estimation of data noise and inverse operator errors distributions parameters, we quantify the uncertainty with the MCMC algorithm by

1. inversion of the extracted modes of the dispersion curves  $\mathbf{W}(\mathbf{V}_R^{extracted}(f)) = \overline{\mathbf{m}}$ ;
2. forward modeling  $\mathbf{F}(\overline{\mathbf{m}}) = \mathbf{V}_R^{restored}(f)$ ;
3. introduction of noise to the dispersion data  $\mathbf{D}_{noised} = \mathbf{V}_R^{restored}(f) + n(f)$  at each frequency, where  $n(f)$  is value generated by the distribution  $N^{noise}(0, \sigma_{noise}(f))$ .

The matrix of corrupted phase velocities,  $\mathbf{D}_{noised}$  has the dimension of  $p \times u$ , where a reasonable amount of  $u$  is 10,000 samples in sense of a statistically significant sample;

4. inversion of the  $\mathbf{D}_{noised}$  matrix:  $\mathbf{W}(\mathbf{D}_{noised}) = \overline{\mathbf{M}}_{noised}$ ;
5. introduction of the inverse operator errors  $\mathbf{M}_{target} = \overline{\mathbf{M}}_{noised} + n$ , where  $n$  is the value generated by the distribution  $N^{error}(\mu_{error}, \sigma_{error})$ . The matrix  $\mathbf{M}_{target}$  has the dimension of  $u \times (2l - 1)$ .

The distribution,  $\mathbf{M}_{target}$  is the matrix of restored velocity model parameters. Each velocity model  $[\mathbf{V}_S, \mathbf{h}]$  from  $\mathbf{M}_{target}$  can be considered a possible 1D S-wave velocity model that is in accordance with the extracted dispersion curves, with provision for introducing the frequency-dependent normally distributed noise to dispersion data and the normally distributed inverse operator errors to the inversion result. We have assumed that both error terms, noise and inversion errors, are Gaussian, but the algorithm implemented in this work can be applied to whatever parametric or non-parametric error distributions. Note that even though the resources to design and train an ANN may be high, once the ANN is trained, the application of the fitted weights to inverse the model parameters is negligibly small and grows insignificant with an increase of the examples number,  $u$ .

## RESULTS

Throughout this section, we demonstrate the application examples of the described above algorithms for inversion and uncertainties quantification during the processing of synthetic and field data. We show three synthetic cases for different velocity models: 1st - is a velocity model with a positive depth gradient (PGV-model), 2nd - is a model

with a low-velocity layer (LVL-model), and 3rd - is a model with a high-velocity layer (HVL-model). During synthetic experiments, we reconstruct the velocity model from the mathematical expectation of the calculated posterior distributions and match it with the true model in two cases: uni-modal (only the fundamental mode is used) and multi-modal (the fundamental mode and the subsequent two higher modes are used) inversion. For a real-data test, engineering seismic data with visually identifiable three modes is used. In this case, the uncertainties for the uni-modal and multi-modal inversion are also estimated. The result is compared with the velocity model, which was obtained with generalized reciprocal method (GRM) for processing of the S-wave first arrival times.

## **Synthetic experiments**

### *Positive gradient velocity model*

For the first synthetic experiment, we chose a four-layer PGV-model (a simulation of a sediment accumulation), which is shown in Figure 4 by the red dotted line. For this model, the first three modes of the Rayleigh surface wave were calculated, which are shown in Figure 5 by a solid line. To obtain a seismogram that contains only calculated Rayleigh surface wave modes, we used the algorithm described by Gaždová and Vilhelm (2011). This algorithm allows calculating the waveforms based on the summation of frequency components, with shifts corresponding to the velocity dispersion and distance. After calculating the waveforms, the end-on spread shot

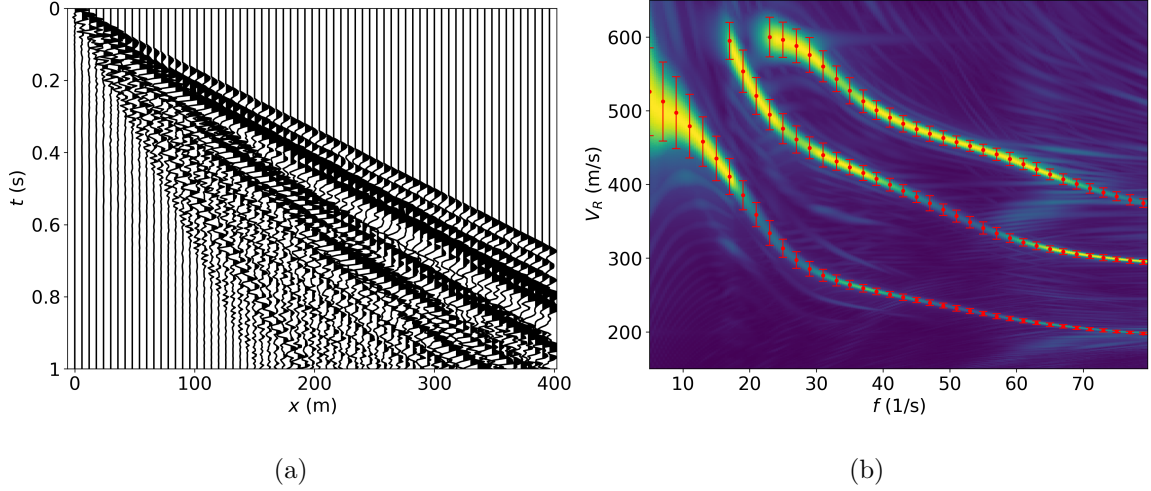


Figure 1: Synthetic seismogram (a) and its  $V - f$  spectra with the confidence intervals of picking shown in red color (b) for PGV-model.

seismogram was gathered (Figure 1a). In a completely similar way, we have calculated synthetic seismograms in other experiments.

Then, we computed the  $V - f$  spectrum (Figure 1b) using the SFK transform and manually picked three modes of the phase velocity dispersion curves. The extracted phase velocities and spectrum amplitudes values are used to determine the range of picking errors (indicated by red confidence intervals in Figure 1b), which limited decreasing of the spectral amplitudes of a mode is twice relative to its maximum at a fixed frequency. Analyzing Figure 1b, we clearly see that the spectral smearing of the energy peaks increases with decreasing frequency and the picking ambiguity range decreases with frequency for each mode.

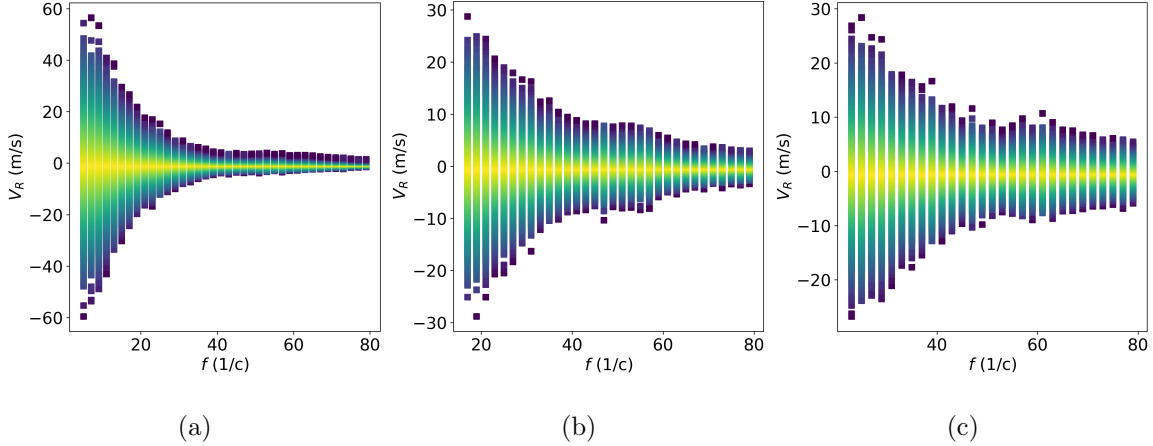


Figure 2: The noise data distributions for fundamental (a), first (b) and second (c) modes extracted from the phase velocity dispersion curves for PGV-model. Color scaling means the interval hit rate, the brighter it is, the more hits it has.

We generate the noise for each mode of the phase velocity, supposing it is Gaussian at each frequency:  $N^{noise}(0, \sigma_{noise}(f))$ . The resulting normal distributions of the added noise  $N^{noise}$  are shown in Figure 2, where the color shows the number of hits in the interval (the brighter the color, the more values this error has). As we can see, the addition of noise to the fundamental mode is more significant (more than two times) than to the higher modes in this case. However, this is not a rule and rather depends on the type of model considered, which will be shown later. Below, we use only the noisy fundamental mode for uni-modal inversion and all three noisy modes for multi-modal inversion.

Only the picked values of the fundamental mode are used to estimate the ranges

(shown by the black dotted lines in Figure 4) of possible values of the reconstructing velocity model parameters according to the inversion algorithm. The training data -  $[\mathbf{V}_S, \mathbf{h}] \in \mathbf{M}^{train}$  and its corresponding  $\mathbf{V}_R^{train} \in \mathbf{D}^{train}$  is calculated within the estimated ranges. For uni-modal inversion, only the fundamental mode is calculated; for multi-modal inversion, the first three modes are calculated. The average computation time for 100,000 dispersion curves is about 20 s for only fundamental mode and about 50 s for the first three modes when using a CPU-parallel solver with OpenMPI and a PC with 32 CPUs AMD Ryzen and 64 Gb RAM. Then we train ANN and use saved weights to invert the train dispersion curves and compute errors  $\mathbf{E}$ . Obtaining mathematical expectation of  $\mathbf{E}$  and standard deviation and assuming Gaussian distributed errors, we estimate inverse operator errors as  $N^{error}(\mu_{error}, \sigma_{error})$ . The resulting normal distributions of the noise additive  $N^{error}$  are shown in Figure 3 for the S-wave velocity and thickness in each layer in cases using only fundamental mode and using the first three modes of the phase velocity.

According to our adaptation of the algorithm for uncertainties quantification, the extracted dispersion curves (only the fundamental modes for the uni-modal and all three modes for the multi-modal case) are inverted using the ANN weights and the 1D velocity model is reconstructed. Then the direct problem is solved, and the phase velocities are calculated using the reconstructed velocity model. Next, to the reconstructed dispersion curve (to the three modes in the multi-modal case), the previously estimated noise  $\mathbf{H}$  is added. Then the stored weights are applied again to invert the noisy dispersion curves, and inverse operator noise is added to the resulting

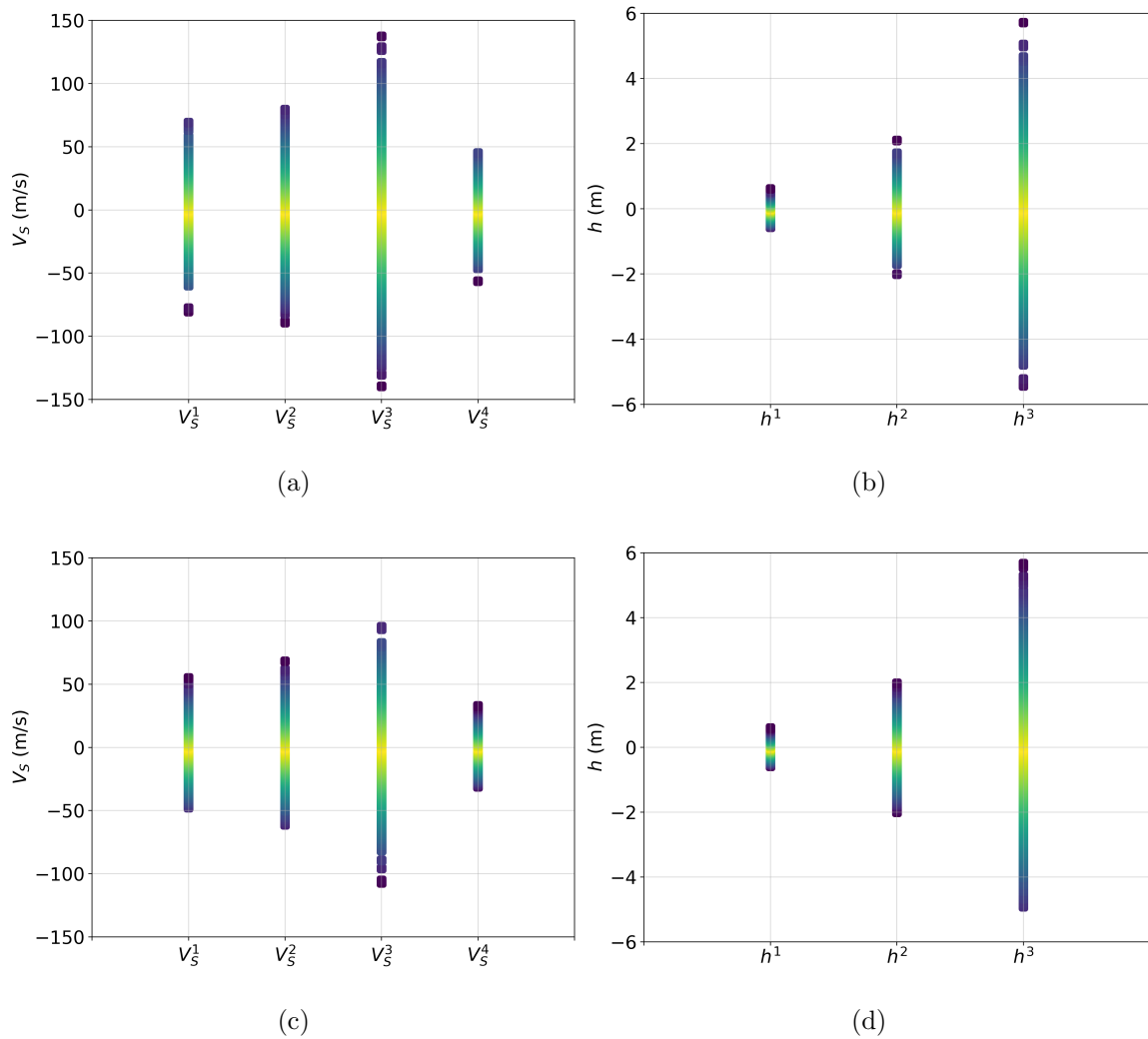


Figure 3: The error distributions of the inverse operator (ANN) using the uni-modal training set for the S-wave velocity (a) and thickness (b) and using the multi-modal training set for the S-wave velocity (c) and thickness (d) The color shows the number of hits in the interval (the brighter the color, the more values this error has) for PGV-model.

velocity models. As a result of the projection of the noise in the data and the errors of the inverse operator, we obtain the posterior distribution of the reconstructed values of the S-wave velocity (Figure 4a for uni-modal and 4c for multi-modal case) and thickness (Figure 4b for uni-modal and 4d for multi-modal case) for each layer. The mathematical expectation of the posterior distribution of S-wave velocity,  $\mu(V_S)$ , and thickness,  $\mu(h)$ , yields the "average model" (shown by gray solid line in Figure 4) - a robust result of solving the inverse problem. The minimum and maximum values of the posterior distribution determine the uncertainties range (shown by gray dashed line in the Figure 4). Maximum absolute errors (MA) between true and average models for uni-modal inversion are  $MA(V_S) = 15 \text{ m/s}$ ,  $MA(h) = 0.4 \text{ m}$ ; for multi-modal inversion are  $MA(V_S) = 1 \text{ m/s}$ ,  $MA(h) = 0.3 \text{ m}$ .

In addition to mathematical expectations  $\mu(V_S)$  and  $\mu(h)$ , we also analyze the next three statistical moments: standard deviation ( $\sigma(V_S)$  and  $\sigma(h)$ ), skewness ( $S(V_S)$  and  $S(h)$ ) and kurtosis ( $K(V_S)$  and  $K(h)$ ). Skewness is a measure of the asymmetry of the distribution. It is customary that if values of skewness are between -0.5 and 0.5, the data are fairly symmetrical. Kurtosis characterizes the "tailedness" of the distribution. Since kurtosis of any univariate normal distribution is 3, we compare computed kurtosis with this value. Computed mathematical expectation and standard deviation for uni-modal and multi-modal inversion were summed in Table 1. The values of skewness of model parameters within the range  $[-0.03; 0.03]$  for both uni- and multi-modal cases. It shows that the distributions are almost perfectly symmetrical. The values of kurtosis within the range  $[2.9; 3.0]$ , that evidence of good conformity to

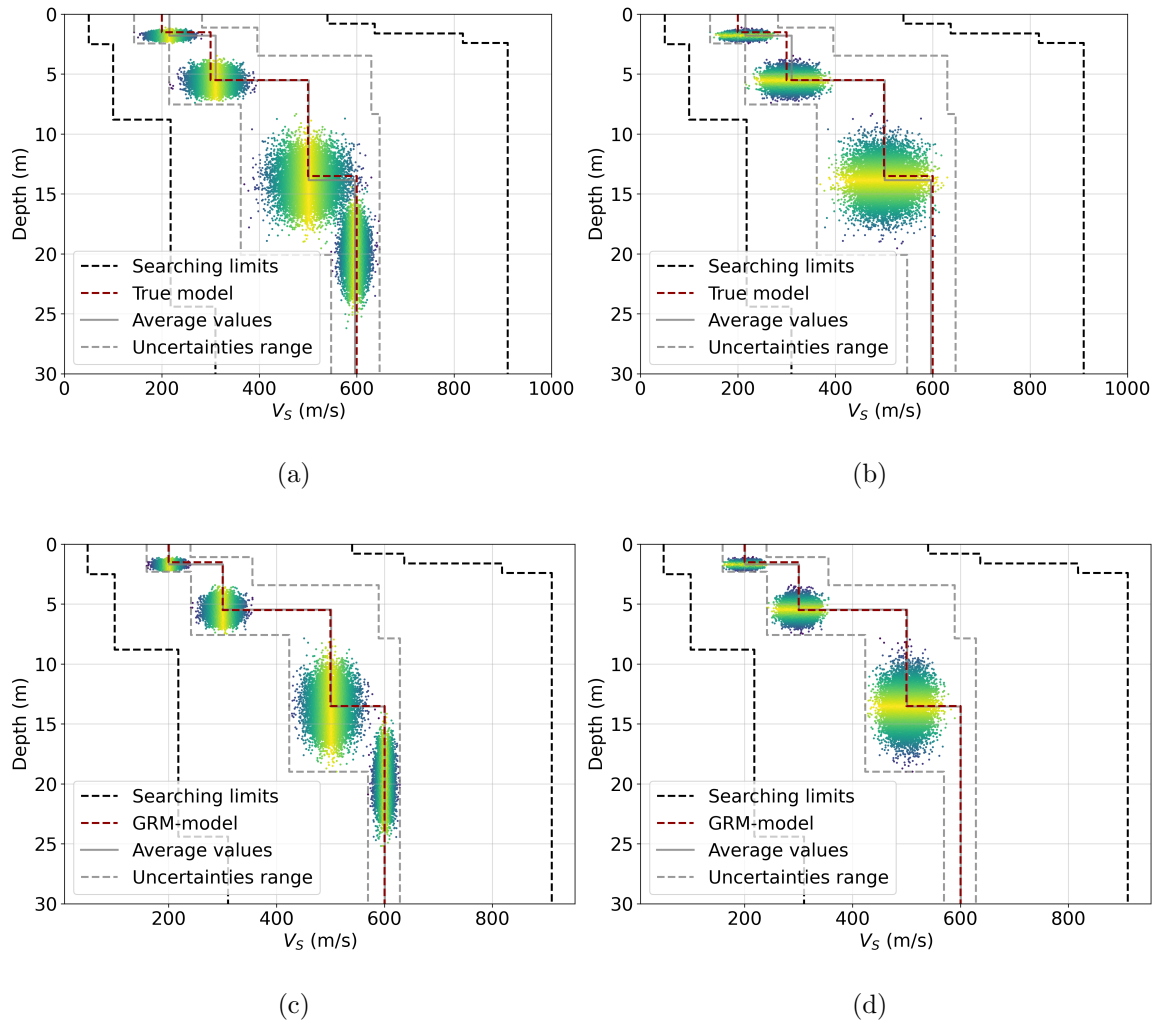


Figure 4: Results of uncertainty quantification for PGV-model: S-wave errors distributions (a) and thickness errors distributions (b) by uni-mode inversion and S-wave errors distributions (c) and thickness errors distributions (d) by multi-mode inversion.

Inversion type	Layer #	S-wave velocity			Thickness		
		True	$\mu(V_S)$	$\sqrt{\sigma(V_S)}$	True	$\mu(h)$	$\sqrt{\sigma(h)}$
Uni- modal	1	200	215	17	1.5	1.8	0.2
	2	300	310	23	4.0	3.7	0.5
	3	500	501	36	8.0	8.4	1.4
	4	600	596	13			
Multi- modal	1	200	201	11	1.5	1.7	0.2
	2	300	301	15	4.0	3.7	0.5
	3	500	501	22	8.0	8.1	1.4
	4	600	600	8			

Table 1: Statistic moment values of the posterior distribution of the model parameters for each layer in the PGV-model’s case.

normal distribution.

We calculated the resulting dispersion curves of the phase velocity using the average velocity model and compared them with the observed ones (Figure 5). The MA between true and average dispersion curves (computed with average velocity model) for uni-modal inversion are  $MA(V_R^1) = 13 \text{ m/s}$ ; for multi-modal inversion are  $MA(V_R^1) = 10 \text{ m/s}$ ,  $MA(V_R^2) = 15 \text{ m/s}$  and  $MA(V_R^3) = 4 \text{ m/s}$  for fundamental, first and second modes, respectively.

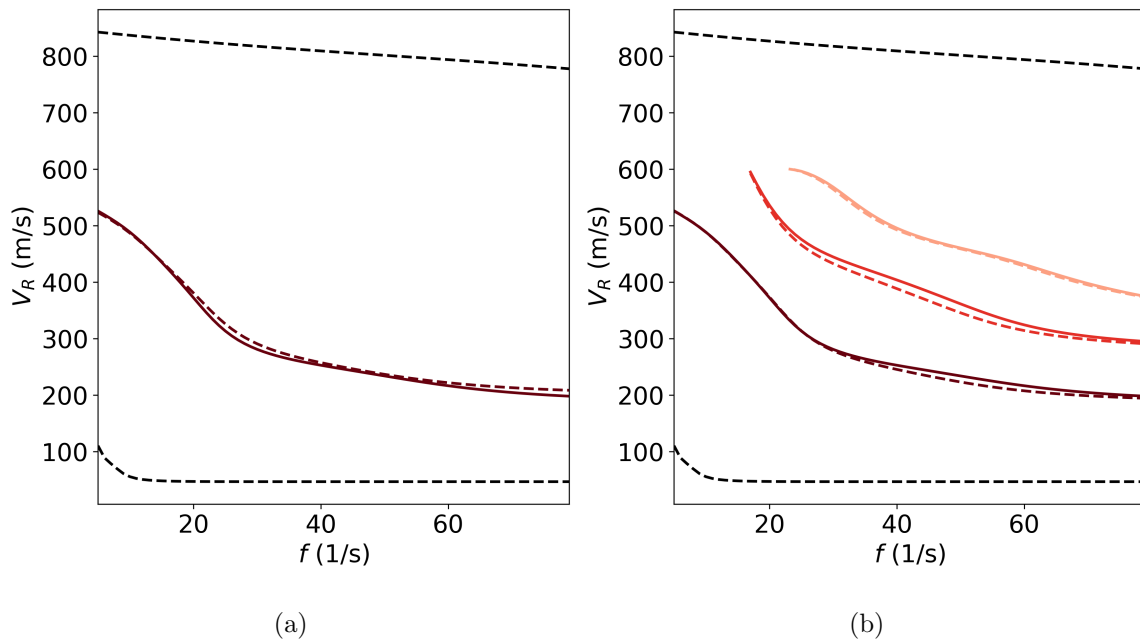


Figure 5: The comparison of the phase velocity dispersion curves computed by average values of uni-mode (a) multi-mode (b) inversion for PGV-model.

### *Low-velocity layer model*

The presence of low-velocity layer (the pavement simulation) leads to the energy redistribution in a spectrum between different modes in various frequency ranges. For example, in our case, we see the decrease of fundamental mode energy and the increase in the energy of the first mode within the range of 15-20 Hz as well as for the first and second modes within the range of 40-50 Hz (Figure 6b). But we also see the back redistribution from the second to the first mode in a range of more than 60 Hz. In the case of the irregular distribution of energy, the picking of dispersion curves becomes even more ambiguous. The energy irregularity in the spectrum may also be caused by the presence of shallow lateral heterogeneous, interference of different seismic waves, regular and random noise. In our case, we have a possibility to exactly extract all modes since we examine noise-free seismogram containing the surface wave only (Figure 6a). Nevertheless, the picking error range (indicated by red confidence intervals in Figure 6b) and, correspondingly, the standard deviation of the Gaussian noise distribution, are decreasing and growing with increasing frequency for higher modes.

In order to quantify the uncertainty for the model with a low-velocity layer, we applied the sequence of operations, which are completely analogous to the previous example. The results of uncertainty quantification for uni-mode (using fundamental curve only) and multi-mode (using the first three modes) inversion are shown in Figure 7. Maximum absolute errors between true and average models for uni-modal inversion are  $MA(V_S) = 5 \text{ m/s}$ ,  $MA(h) = 1.1 \text{ m}$ ; for multi-modal inversion are

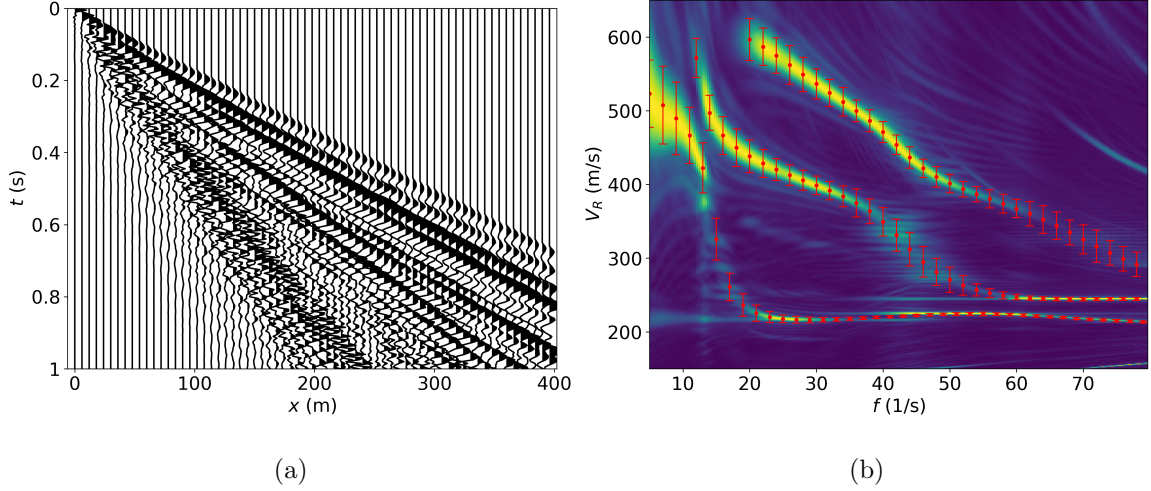


Figure 6: Synthetic seismogram (a) and its  $V - f$  spectra with the confidence intervals of picking shown in red color (b) for LVL-model.

$$\text{MA}(V_S) = 5 \text{ m/s}, \text{MA}(h) = 0.8 \text{ m}.$$

Computed mathematical expectation and standard deviation for uni-modal and multi-modal inversion are listed in Table 2. The values of skewness of model parameters are within the range  $[-0.02; 0.06]$  for both uni- and multi-modal cases. It shows that the distributions are almost perfectly symmetrical. The values of kurtosis within the range  $[2.9; 3.1]$ , that evidence of good conformity to normal distribution.

The MA between true and average dispersion curves (computed with average velocity model) for uni-modal inversion is  $\text{MA}(V_R^1) = 91 \text{ m/s}$ ; for multi-modal inversion are  $\text{MA}(V_R^1) = 38 \text{ m/s}$ ,  $\text{MA}(V_R^2) = 18 \text{ m/s}$  and  $\text{MA}(V_R^3) = 7 \text{ m/s}$  for fundamental, first and second modes, respectively.

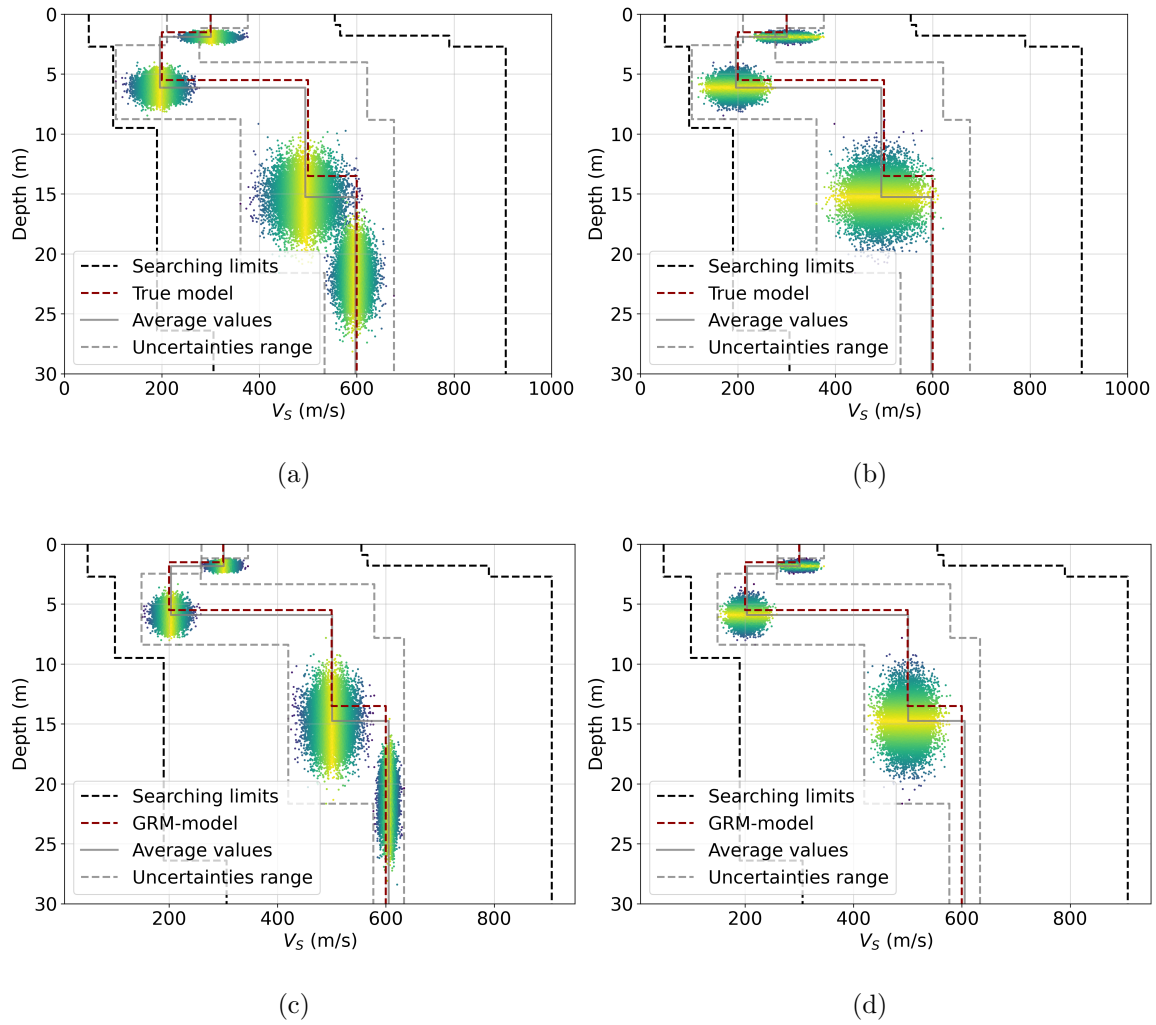


Figure 7: Results of uncertainty quantification for LVL-model: S-wave errors distributions (a) and thickness errors distributions (b) by uni-mode inversion and S-wave errors distributions (c) and thickness errors distributions (d) by multi-mode inversion.

Inversion type	Layer #	S-wave velocity			Thickness		
		True	$\mu(V_S)$	$\sqrt{\sigma(V_S)}$	True	$\mu(h)$	$\sqrt{\sigma(h)}$
Uni-modal	1	300	301	21	1.5	1.9	0.2
	2	200	196	22	4.0	4.2	0.6
	3	500	495	36	8.0	9.1	1.5
	4	600	597	18			
Multi-modal	1	300	301	12	1.5	1.8	0.2
	2	200	203	14	4.0	4.1	0.6
	3	500	501	23	8.0	8.8	1.4
	4	600	605	8			

Table 2: Statistic moment values of the posterior distribution of the model parameters for each layer in the LVL-model’s case.

*High-velocity layer model*

The seismogram containing only three modes of Rayleigh surface wave for the third synthetic example is shown in Figure 8a. The presence of a high-velocity layer (the permafrost simulation) leads to energy redistribution in a spectrum much more than the previous example (Figure 8b). In this case, we see the decreasing of the fundamental mode energy within several frequency ranges: 8-12 Hz, 18-37 Hz, and 45-80 Hz. It leads to irregular decreasing and increasing picking error range (indicated by red confidence intervals in Figure 8b) for all existing modes.

The results of uncertainty quantification for uni-mode (using fundamental curve only) and multi-mode (using the first three modes) inversion are shown in Figure 9.

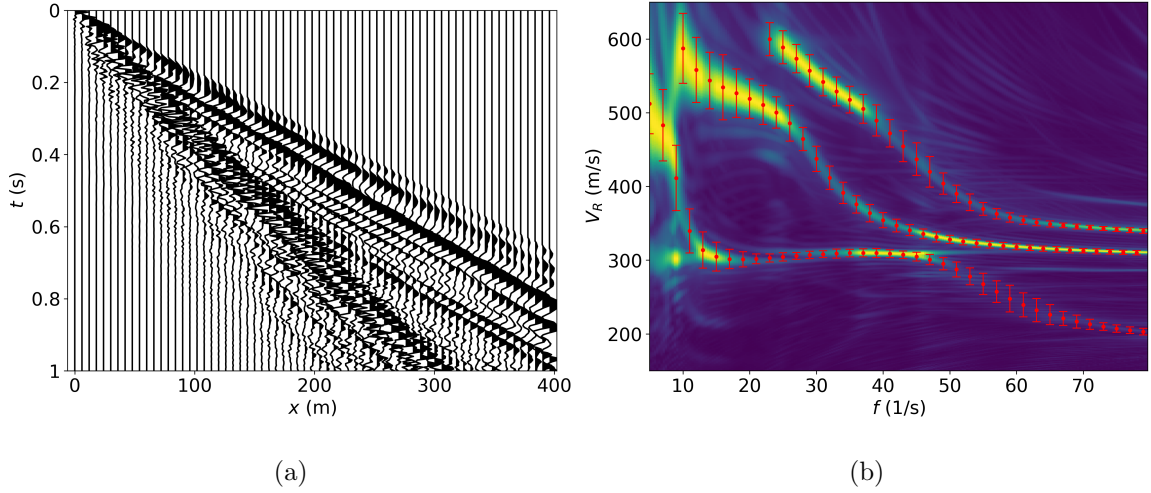


Figure 8: Synthetic seismogram (a) and its  $V - f$  spectra with the confidence intervals of picking shown in red color (b) for HVL-model.

Maximum absolute errors between true and average models for uni-modal inversion are  $MA(V_S) = 27 \text{ m/s}$ ,  $MA(h) = 1.8 \text{ m}$ ; for multi-modal inversion are  $MA(V_S) = 6 \text{ m/s}$ ,  $MA(h) = 1 \text{ m}$ .

Computed mathematical expectation and standard deviation for uni-modal and multi-modal inversion were summed in Table 3. The values of skewness of model parameters are within the range  $[-0.07; 0.04]$  for both uni- and multi-modal cases. It shows that the distributions are almost perfectly symmetrical. The values of kurtosis within the range  $[3.0; 3.1]$  what give an evidence of a good conformity to the normal distribution.

The MA between true and average dispersion curves (computed with average ve-

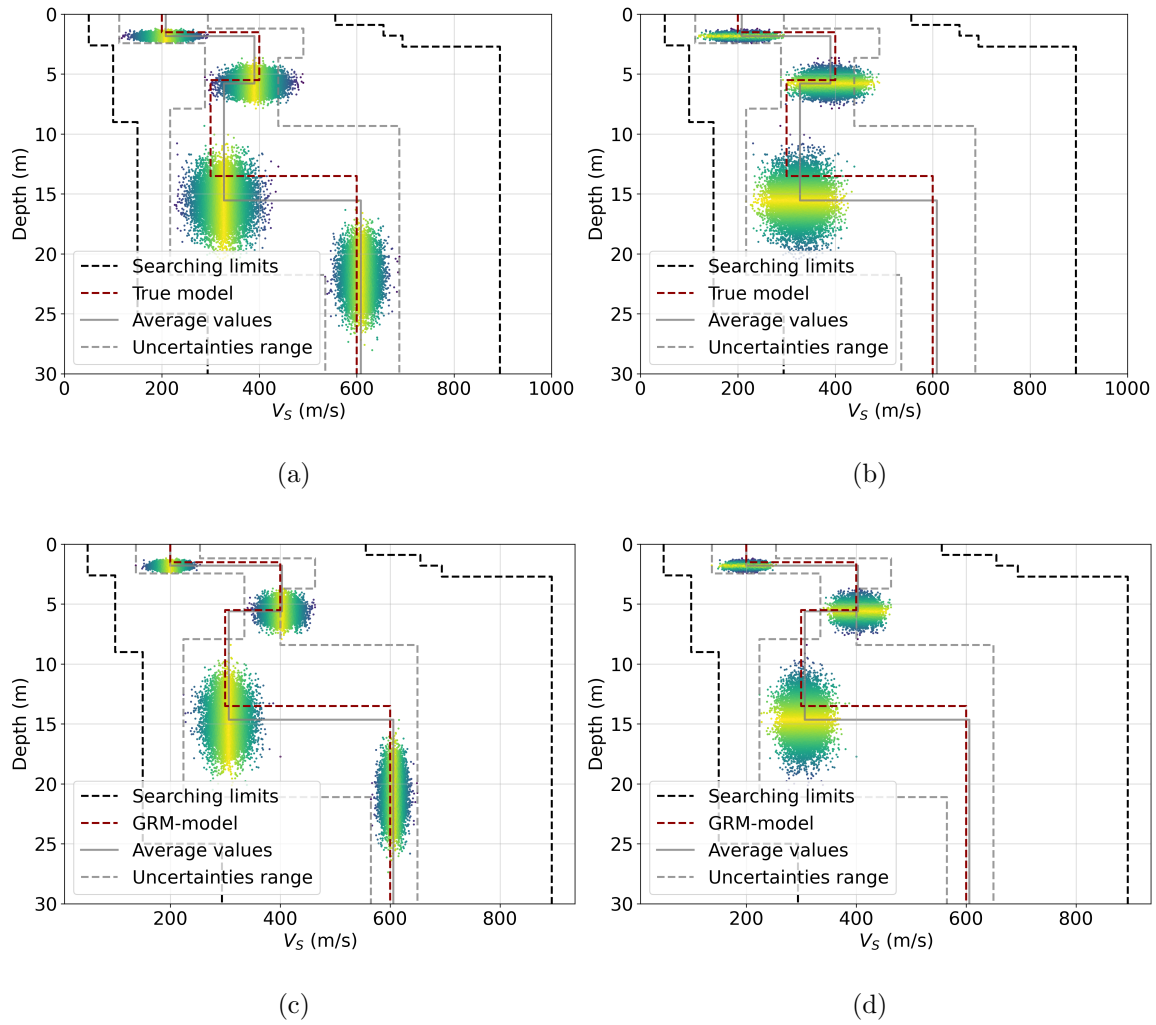


Figure 9: Results of uncertainty quantification for HVL-model: S-wave errors distributions (a) and thickness errors distributions (b) by uni-mode inversion and S-wave errors distributions (c) and thickness errors distributions (d) by multi-mode inversion.

Inversion type	Layer #	S-wave velocity			Thickness		
		True	$\mu(V_S)$	$\sqrt{\sigma(V_S)}$	True	$\mu(h)$	$\sqrt{\sigma(h)}$
Uni- modal	1	200	208	24	1.5	1.8	0.2
	2	400	390	28	4.0	3.9	0.5
	3	300	327	31	8.0	9.8	1.4
	4	600	609	20			
Multi- modal	1	200	200	14	1.5	1.8	0.2
	2	400	403	17	4.0	3.8	0.5
	3	300	306	21	8.0	9.0	1.4
	4	600	606	11			

Table 3: Statistic moment values of the posterior distribution of the model parameters for each layer in the HVL-model’s case.

locity model) for uni-modal inversion is  $MA(V_R^1) = 41 \text{ m/s}$ ; for multi-modal inversion are  $MA(V_R^1) = 48 \text{ m/s}$ ,  $MA(V_R^2) = 30 \text{ m/s}$  and  $MA(V_R^3) = 62 \text{ m/s}$  for fundamental, first and second modes, respectively.

## Field data processing

The field data were acquired in the vicinity of Novosibirsk, Russia. The linear acquisition system was used and consisted of 30 triaxial (3C) geophones with a sampling frequency of 10 Hz placed with 5 m spacing. The length of seismic profile is 145 m. The time-domain acquisition parameters were 2 s length and 1ms sampling rate.

Horizontal hits with a sledgehammer of 5 kg by loaded railway sleeper were used

for the generation of S-waves. Hits were carried out for both sides of the sleeper, then recorded seismograms were subtracted from each other to increase S-wave and decrease P-wave. An example of a recorded seismogram of horizontal displacement velocity with horizontal source type is shown in Figure 10a.

A 100 kg dropped weight from 2 m height was used to generate P-waves. An example of a recorded seismogram of vertical displacement velocity with vertical source type (z-z seismogram) is shown in Figure 10b.

Let's compare y-y and z-z seismograms for the first shot point at 0 m (shown by black lines in Figure 10a) and the end shot point at 145 m (shown by red lines in Figure 10a). Note that the first arrivals are close for forward (0 m) and back (145 m) seismograms as well as for z-z seismograms (Figure 10b), which indicate the sub-horizontal velocity structure of the subsurface. We reconstructed the 1D velocity S-wave velocity model using the y-y seismograms processing with the generalized reciprocal method (GRM) (Palmer, 1981). The obtained S-wave velocity model by the GRM is shown in Figure 12 by red dashed lines.

To reconstruct the 1D S-wave velocity profile by the MASW method, we use a full seismogram for vertical displacement with a vertical source containing multi-modal Rayleigh wave (Figure 11a). As can be seen from the phase velocity spectrum (Figure 11b) the Rayleigh wave contains at least three modes. We do not have confidence in the fourth mode since its presence might be connected with an aliasing effect. Nevertheless, we clearly see three modes (fundamental and two high order modes) of a simple form without an energy redistribution in a spectrum, which indicates a quiet

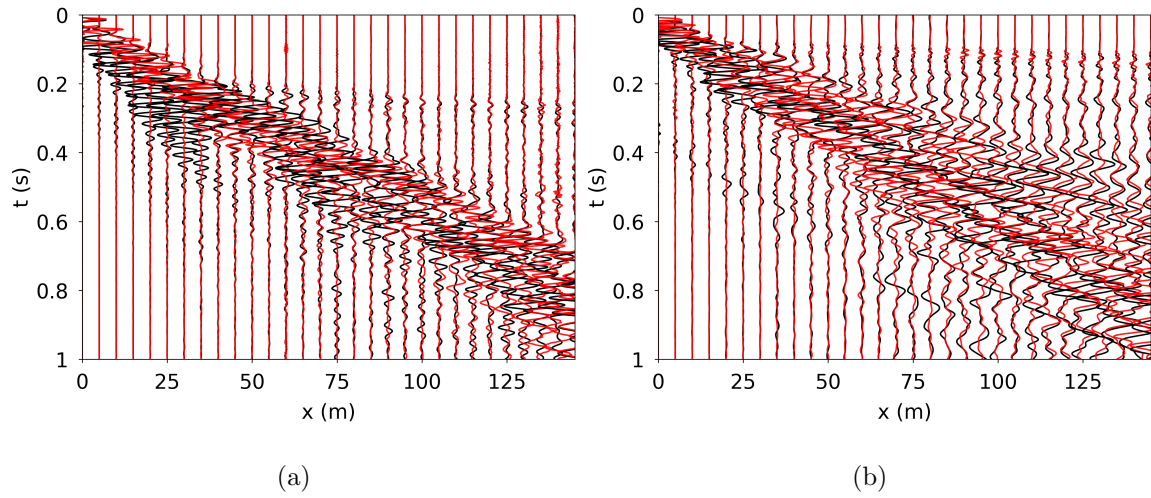


Figure 10: Field seismogram (y-y) of horizontal velocity displacement with using corresponding horizontal source for waves generation (a) and field seismogram (z-z) of vertical velocity displacement with using corresponding vertical source (b). Seismograms for source 0 m (first point of the seismic profile) and source 145 m (end point of the seismic profile) are shown in black and red colors, respectively

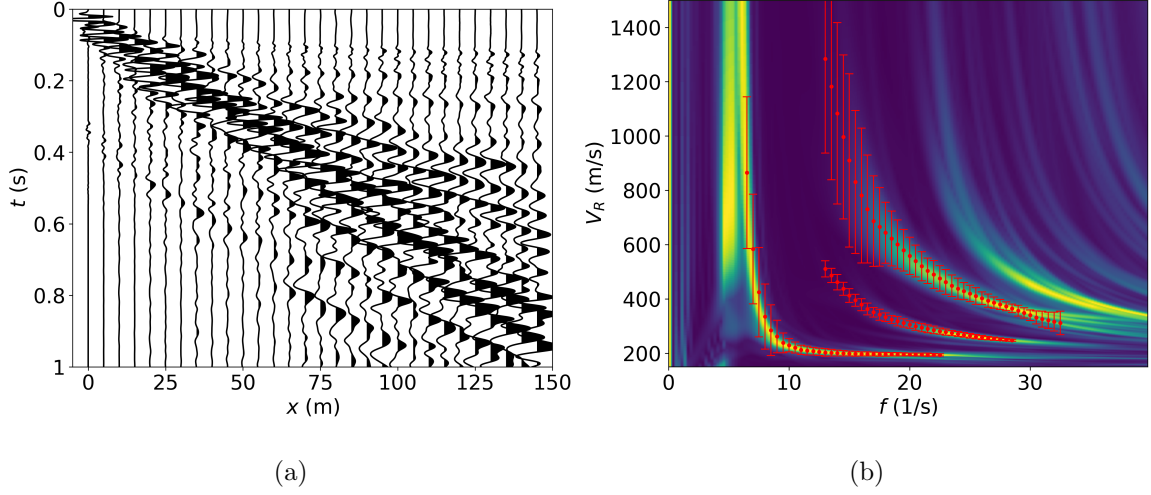


Figure 11: Field seismogram ( $z$ - $z$ ) of vertical velocity displacement with using vertical source for waves generation (a) and its  $V - f$  spectra with the confidence intervals of picking shown in red color (b).

sediment accumulation condition.

Similar to the synthetic examples, picking errors are estimated with a double attenuation of amplitude in relation to its maximum at each frequency for each unidentified mode. The difference between training and predicted model parameters by ANN gives the distribution of inversion operator errors. Applying the mentioned algorithm of Monte-Carlo simulation, we determine PPDs of restored S-wave velocity and thickness values, which statistic yields an estimation of uncertainties ranges. As in previous examples, we examine uni-modal (using fundamental mode only) and multi-mode (using the first three modes) inversions. The resulting PPDs are shown in Figure 12.

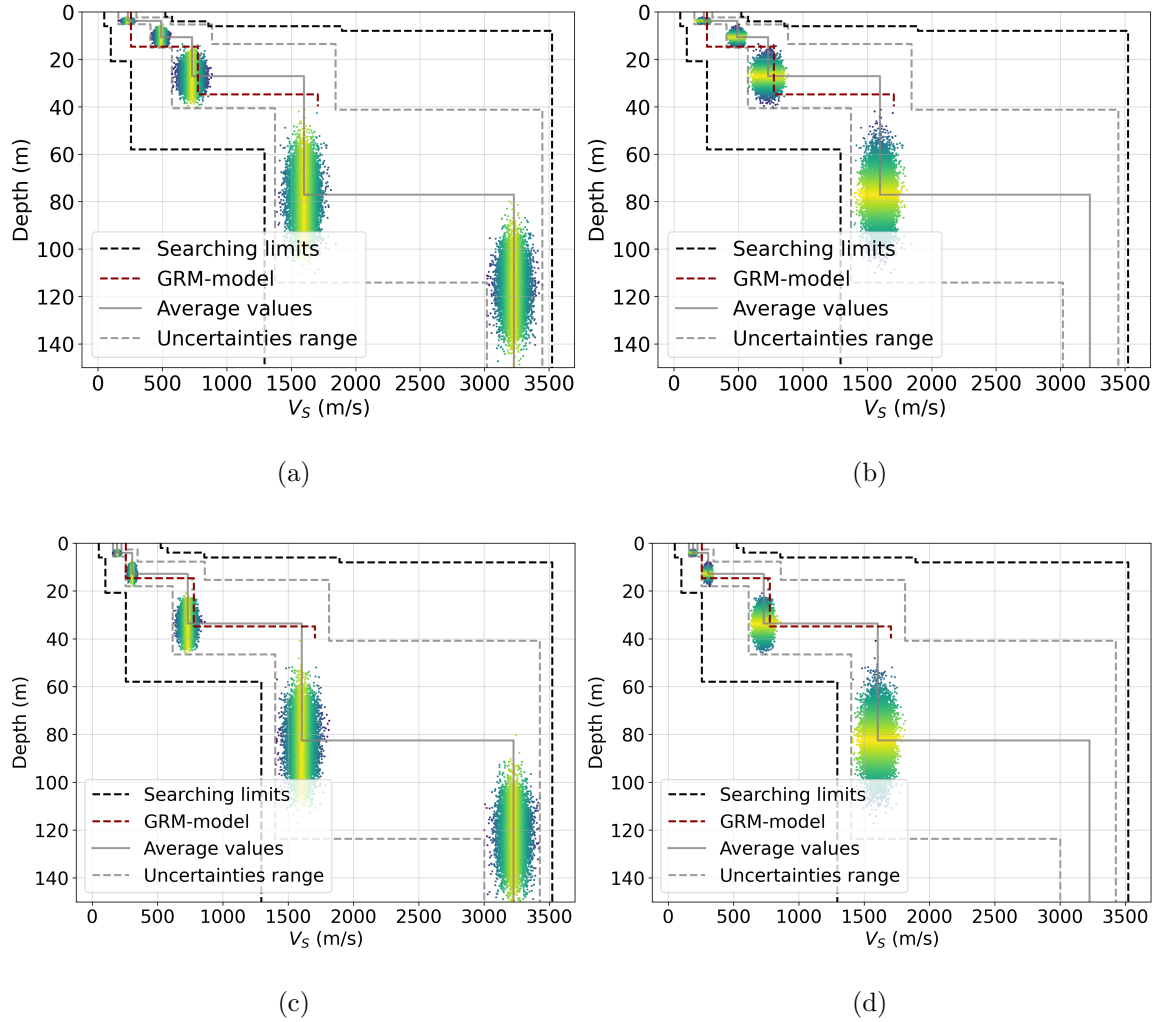


Figure 12: Results of uncertainty quantification while field data processing: S-wave errors distributions (a) and thickness errors distributions (b) by uni-mode inversion and S-wave errors distributions (c) and thickness errors distributions (d) by multi-mode inversion.

We again observe that the uncertainty of S-wave velocity and thickness increase as the depth of the considered layer increases. We observe the well predicted velocities matching with GRM velocities in both uni-modal and multi-modal cases. However, multi-modal case yields better matching in thicknesses. Also, we observe that the MASW gives a more detailed 1D model - there is an additional shallow layer and the model is deeper with comparison to the GRM model.

The comparison of the modes computed by the average models of PPDs and extracted ones from the data shows the well matching in the considered frequency range: mean absolute error for uni-modal inversion is  $\text{MAE}(V_R^1) = 41 \text{ m/s}$ ; for multi-modal inversion are  $\text{MAE}(V_R^1) = 55 \text{ m/s}$ ,  $\text{MAE}(V_R^2) = 29 \text{ m/s}$  and  $\text{MAE}(V_R^3) = 39 \text{ m/s}$  for fundamental, first and second modes, respectively. Therefore, we consider that the final predictions are in agreement with the observed data and with the assumed noise and inverse operator errors.

## DISCUSSIONS

Special attention in our study is given to comparison of the uncertainty ranges of uni-modal and multi-modal inversion. It follows from the results that in the multi-modal case, the PPD's expectation is closer to the true values of the model parameters, and the PPD's standard deviation is much smaller than in the uni-modal case. It is especially noticeable for the models with close velocities in adjacent layers. For example, experiments with the positive gradient velocity model and LVL-model show that when only the fundamental mode is used, the uncertainty ranges of the velocity

in the 3rd and 4th layers intersect, i.e. some resulting models have the equal velocity in the 3rd and 4th layers (confer Figures 4a and 7a). This leads to skipping the 3rd interface, which can be significant, for example, in problems of micro-seismic zoning. In contrast, in case of the multimodal inversion, the velocities in the neighboring layers are well separated, and the 3rd boundary is restored (confer Figures 4c and 7c). However, our experiments do not show a decrease of the PPD's standard deviation for thicknesses, which may be due to the low sensitivity of the first two high order modes used in this work to thickness changes. An additional analysis of the sensitivity of high order modes and their individual parts to changes in thickness is required and will be done in the future.

Another interesting observation is connected to the redistribution of energy between the modes which affects the inversion uncertainty significantly. This is because the energy outflow increases the ambiguity range of the dispersion curves peaking. The energy outflow in the spectra is observed when the velocity gradient changes its sign with depth. This can be easily illustrated for the HVL-model, where there is energy outflow from the fundamental mode in the range of 50-70 Hz (Figure 8b). This leads to a wider range of uncertainty of the 1st layer velocity (Figure 9a) compared to the result for the LVL-model (Figure 7a), for which there is no energy outflow at these frequencies (Figure 6b).

During the study, it was noticed that for multi-modal inversion with a large number of training epochs, steps may appear on the learning curves - a sharp decrease in the value of the misfit function between neighbor epochs. This is mainly due to the

fact that the optimization algorithm reduces the learning rate when the loss function plateaus. It appears, in our example, when using the Nadam algorithm with an adaptive learning rate. With uni-modal inversion, no such steps were observed. When the number of training epochs increases (tested 100 and 300 epochs) with uni-modal inversion, the uncertainties ranges decrease slightly, but with multi-modal inversion, the uncertainties ranges decrease significantly, while everything else remains equal. Perhaps because the objective functional surface is more complex when using numerous modes, and training is smoother, and we reach a deeper global minimum than when using a single mode. When using one mode, the global minimum is not reached even with a large number of epochs and training falls into a local minimum. Thus, when using multi-modal inversion, it is advisable to increase the number of training epochs to get a better result.

Let's summarize the main factors of computational effectiveness carried out experiments. The average computation time for 100,000 dispersion curves is about 20 s for only fundamental mode and about 50 s for the first three modes when using a CPU-parallel solver with OpenMPI and a PC with 32 CPUs AMD Ryzen and 64 Gb RAM. The average ANN training time is about 330 s when using a program implementation based on the Keras Python library and a PC with GeForce GTX 1080 Ti. The average time of the ANN with the predetermined weights is about 0.5 s for inverting of the 10,000 examples. This time grows insignificant with increasing of the examples number ( $u$  in our notation).

An advantage of the proposed algorithm is the fact that once the ANN has been

trained, it provides predictions of the S-wave velocity model and related uncertainties in real-time without extra computational cost.

## CONCLUSION

We improved previous uni-modal (Yablokov et al., 2021) to multi-modal approach. The advantage of multi-modal inversion over uni-modal is confirmed by the comparison between PPDs of the velocity model parameters. Estimated PPDs are a result of uncertainties quantification, which takes into account data noise and inverse operator errors. The mathematical expectations of the estimated PPDs are robust assessments of velocity structure in comparison with a standard approach because it provides statistical characteristics. The use of ANN is valid due to the low computational cost, since the inverse problem has to solve many times for an accurate estimation of PPD. Moreover, the proposed approach does not include any constraint into the misfit function different from standard inversion approaches. The ANN is trained on a dataset containing realistic models and learns how to reproduce a model to fit the dispersion curve. At the preparation stages of the proposed algorithm, the reasonable layers number and the ranges of possible values of the velocity model parameters are determined from the reference observed dispersion curve. Then the ANN is trained. Once trained, the ANN for a fixed number of layers can be used for the entire study area.

We proposed an approach to restore the 1D S-wave velocity model with its uncertainty quantification (each layer's S-wave velocity and thickness values) by multi-modal inversion of the surface wave dispersion data using a hybrid ANN and Monte

Carlo simulation strategy. Synthetic and field experiments have demonstrated high-potential results - using ANN yields the possibility to accurately estimate PPD of restored model parameters without a significant computational effort. Also, the multi-mode inversion domination over uni-modal confirms with the comparison its estimated PPD. The trained ANN provides reasonable model parameters predictions and related uncertainties in real-time.

## REFERENCES

- Aleardi, M., and A. Salusti, 2021, Elastic pre-stack inversion through discrete cosine transform reparameterization and convolutional neural networks: *Geophysics*, **86**, 1JF–V89.
- Aleardi, M., A. Salusti, and S. Pierini, 2020, Transdimensional and hamiltonian monte carlo inversions of rayleigh-wave dispersion curves: a comparison on synthetic datasets: *Near Surface Geophysics*, **18**, 515–543.
- Aleardi, M., and E. Stucchi, 2021, A hybrid residual neural network–monte carlo approach to invert surface wave dispersion data: *Near Surface Geophysics*, **19**, 397–414.
- Beaty, K. S., D. R. Schmitt, and M. Sacchi, 2002, Simulated annealing inversion of multimode rayleigh wave dispersion curves for geological structure: *Geophysical Journal International*, **151**, 622–631.
- Cao, R., S. Earp, S. A. de Ridder, A. Curtis, and E. Galetti, 2020, Near-real-time near-surface 3D seismic velocity and uncertainty models by wavefield gradiometry and neural network inversion of ambient seismic noise: *Geophysics*, **85**, KS13–KS27.
- Çaylak, Ç., and İ. Kaftan, 2014, Determination of near-surface structures from multi-channel surface wave data using multi-layer perceptron neural network (mlpnn) algorithm: *Acta Geophysica*, **62**, 1310–1327.
- Comina, C., S. Foti, D. Boiero, and L. Socco, 2011, Reliability of vs<sub>30</sub> evaluation from surface-wave tests: *Journal of Geotechnical and Geoenvironmental engineer-*

- ing, **137**, 579–586.
- Cox, B. R., and D. P. Teague, 2016, Layering ratios: a systematic approach to the inversion of surface wave data in the absence of a priori information: *Geophysical Journal International*, **207**, 422–438.
- Foti, S., C. Comina, D. Boiero, and L. Socco, 2009, Non-uniqueness in surface-wave inversion and consequences on seismic site response analyses: *Soil Dynamics and Earthquake Engineering*, **29**, 982–993.
- Foti, S., C. G. Lai, G. J. Rix, and C. Strobbia, 2014, *Surface wave methods for near-surface site characterization*: CRC press.
- Gaždová, R., and J. Vilhelm, 2011, Diseca—a matlab code for dispersive waveform calculations: *Computers and Geotechnics*, **38**, 526–531.
- Herrmann, R. B., 2013, Computer programs in seismology: An evolving tool for instruction and research: *Seismological Research Letters*, **84**, 1081–1088.
- Kurita, T., 1973, Regional variations in the structure of the crust in the central united states from p-wave spectra: *Bulletin of the Seismological Society of America*, **63**, 1663–1687.
- Lai, C. G., S. Foti, and G. J. Rix, 2005, Propagation of data uncertainty in surface wave inversion: *Journal of Environmental & Engineering Geophysics*, **10**, 219–228.
- Luo, Y., J. Xia, J. Liu, Q. Liu, and S. Xu, 2007, Joint inversion of high-frequency surface waves with fundamental and higher modes: *Journal of Applied Geophysics*, **62**, 375–384.
- Maraschini, M., F. Ernst, S. Foti, and L. V. Socco, 2010, A new misfit function for multimodal inversion of surface waves: *Geophysics*, **75**, G31–G43.

- Marosi, K. T., and D. R. Hiltunen, 2004, Characterization of spectral analysis of surface waves shear wave velocity measurement uncertainty: *Journal of geotechnical and geoenvironmental engineering*, **130**, 1034–1041.
- Miller, R. D., J. Xia, C. B. Park, and J. M. Ivanov, 1999, Multichannel analysis of surface waves to map bedrock: *The Leading Edge*, **18**, 1392–1396.
- Molnar, S., S. E. Dosso, and J. F. Cassidy, 2010, Bayesian inversion of microtremor array dispersion data in southwestern british columbia: *Geophysical Journal International*, **183**, 923–940.
- Palmer, D., 1981, An introduction to the generalized reciprocal method of seismic refraction interpretation: *Geophysics*, **46**, 1508–1518.
- Park, C. B., R. D. Miller, and J. Xia, 1999, Multichannel analysis of surface waves: *Geophysics*, **64**, 800–808.
- Serdyukov, A. S., A. V. Yablokov, A. A. Duchkov, A. A. Azarov, and V. D. Baranov, 2019, Slant f-k transform of multichannel seismic surface wave data: *Geophysics*, **84**, A19–A24.
- Song, X., L. Tang, S. Zhao, X. Zhang, L. Li, J. Huang, and W. Cai, 2015, Grey wolf optimizer for parameter estimation in surface waves: *Soil Dynamics and Earthquake Engineering*, **75**, 147–157.
- Supranata, Y. E., M. E. Kalinski, and Q. Ye, 2007, Improving the uniqueness of surface wave inversion using multiple-mode dispersion data: *International Journal of Geomechanics*, **7**, 333–343.
- Xia, J., R. D. Miller, C. B. Park, and G. Tian, 2003, Inversion of high frequency surface waves with fundamental and higher modes: *Journal of Applied Geophysics*,

**52**, 45–57.

Yablokov, A., and A. Serdyukov, 2020, Inversion of surface waves dispersion curves using artificial neural network: 82nd EAGE Annual Conference & Exhibition, European Association of Geoscientists & Engineers, 1–5.

Yablokov, A. V., A. S. Serdyukov, G. N. Loginov, and V. D. Baranov, 2021, An artificial neural network approach for the inversion of surface wave dispersion curves: *Geophysical Prospecting*, **69**, 1405–1432.

Zhang, S. X., and L. S. Chan, 2003, Possible effects of misidentified mode number on rayleigh wave inversion: *Journal of Applied Geophysics*, **53**, 17–29.